

Unsteady hybrid nanofluid flow over a convectively heated cylinder with inclined magnetic field and viscous dissipation: A multiple regression analysis

Bidyasagar Kumbhakar ^{a,*}, Susmay Nandi ^b, Ali J. Chamkha ^c

^a Department of Mathematics, National Institute of Technology Meghalaya, Shillong 793003, India

^b Department of Mathematics, University of Petroleum & Energy Studies, Dehradun 248007, India

^c Faculty of Engineering, Kuwait College of Science and Technology, Doha District, 35004, Kuwait

ARTICLE INFO

Keywords:

Convective heating
Hybrid nanofluid
Lorentz force
Thermal radiation
Unsteady flow
Velocity slip
Viscous dissipation

ABSTRACT

The current study explores the aspects of unsteady stagnation point flow of hybrid nanofluid (Cu-Al₂O₃/H₂O) over a continuously moving and convectively heated stretching cylinder under the influence of oblique Lorentz force. The impacts of velocity slip, Joule dissipation, thermal radiation, viscous dissipation and internal heat generation are also incorporated into this study. Appropriate thermo-physical relations for the hybrid nanofluid are accomplished by following the Xue model. With the use of suitable similarity transformations, the governing dimensional mathematical equations are converted into dimensionless forms. Numerical solutions are obtained for the velocity and energy fields with the help of a shooting technique based on the Runge–Kutta–Fehlberg method of 5-th order and secant iteration. Graphical and tabular representations of numerical data are used to explore the physical impacts of various pertinent parameters on the hybrid nanofluid velocity and temperature. The stability of this approach and the validity of the obtained results are illustrated by comparing the current findings to previously reported data for a specific case. Further, the multiple (quadratic) regression analysis is performed to show the dominance of physical parameters on local skin-friction coefficient and Nusselt number. The thermal buoyancy force boosts the fluid flow while a reverse trend is observed for the magnetic and the velocity slip parameters. Heat transfer rate at the surface is improved with the enhancement in Biot number, thermal radiation and unsteadiness parameters.

1. Introduction

Nanofluid is a homogeneous mixture of very tiny particles of size 10^{-9} m and a base fluid. Generally, metals such as Al, Cu, Ag, TiO₂, Al₂O₃, etc. are used as nanoparticles that are suspended in base fluids like water, methanol, ethylene glycol, oil and to name a few. The metal particles' specific heat is relatively low compared to water or other liquids. Because of this fact, the insertion of nanoparticles in the base fluid improves the thermal conductivity of the working fluid and thereby enhances the rate of heat transfer [1]. Nowadays, numerous engineering, industrial and biological applications of nanofluids can be observed worldwide. Nanofluids are widely used in nuclear reactor and airplanes as coolants, for the treatment of cancer, etc. (see, Refs. [2,3]). Time-dependent

* Corresponding author.

E-mail address: bkmath@nitm.ac.in (B. Kumbhakar).

<https://doi.org/10.1016/j.cjph.2022.07.003>

Received 4 January 2022; Received in revised form 4 July 2022; Accepted 5 July 2022

Available online 8 July 2022

0577-9073/© 2022 The Physical Society of the Republic of China (Taiwan). Published by Elsevier B.V. All rights reserved.

Nomenclature

u, v	Velocity components along x and r directions (m s^{-1})
t	Time (s)
B_1	Constant magnetic field (Tesla)
g	Gravitational acceleration (m s^{-2})
T	Temperature (K)
T_∞	Ambient temperature (K)
k	Thermal conductivity ($\text{W m}^{-1} \text{K}^{-1}$)
c_p	Specific heat at uniform pressure ($\text{J kg}^{-1} \text{K}^{-1}$)
N_2	Velocity slip coefficient
h_2	Constant heat transfer coefficient of convective heat transfer ($\text{W m}^{-2} \text{K}^{-1}$)
L	Characteristic length (m)
A	Unsteadiness parameter
M	Magnetic parameter
N	Thermal radiation parameter
Pr	Prandtl number
Ec	Eckert number
Re_x	Local Reynold number
k^*	Mean absorption coefficient (m^{-1})
q_r	Radiative heat flux (W m^{-2})
Q_1	Constant heat generation coefficient
R	Radius of cylindrical sheet (m)
T_0	Reference temperature (K)
Gr	Thermal Grashof number

Greek Symbols

μ	Dynamic viscosity ($\text{kg m}^{-1} \text{s}^{-1}$)
ϕ	Inclined angle
ρ	Density (kg m^{-3})
σ	Electrical conductivity (S m^{-1})
γ	Biot number
β	Thermal expansion coefficient
β_1	Curvature parameter
ν	Kinematic viscosity ($\text{m}^2 \text{s}^{-1}$)
σ^*	Stefan–Boltzmann constant ($\text{W m}^{-2} \text{K}^{-4}$)
θ	Dimensionless temperature
η	Similarity variable
λ_1	Velocity ratio parameter
Φ_1	Nanoparticle volume fractions for alumina (Al_2O_3)
Φ_2	Nanoparticle volume fractions for copper (Cu)
δ	Velocity slip parameter

Subscripts

bf	Base fluid
nf	Nanofluid
hnf	Hybrid nanofluid
n_1	First nanoparticle
n_2	Second nanoparticle

nanofluid flow generated by a heated surface with heat and mass transport was numerically solved by Hashim et al. [4]. Hybrid nanofluids are a subset of nanofluids. In this special kind of nanofluid, more than one nanoparticle is suspended in the base fluid. This type of fluid has exceptionally good thermal properties compared to normal nanofluid containing a single type of nanoparticles and base liquid. Hybrid nanofluids have found profound use in various sectors, including heat exchangers, vehicle radiators, heating

operations and electronic cooling, nuclear trons, and many more. A significant amount of research studies related to the hybrid nanofluid flow can be found in Dinarvand et al. [5], Waini et al. [6], Aly and Pop [7], Arani and Aberoumand [8], Waini et al. [9].

Magneto-hydrodynamics (MHD) is the combination of electromagnetism properties with fluid flow dynamics. More specifically, it is a noble way of capturing electrically conducting fluid flow activities in the presence of magnetic fields. As a result, in many engineering and technical domains, the flow and heat transfer mechanism for an MHD viscous fluid has received much attention in science and technology. Some applications are found in petroleum extractions, MHD power generators, geothermal energy extractions, nuclear reactor cooling, configuration and orientation of the boundary layer structure, etc. [10]. The relevant research articles unwrapping the impacts of magnetic field are due to Ghadikolaei et al. [11], Hamid et al. [12], Zainal et al. [13], Jamaludin et al. [14], Zainal et al. [15], Srinivasulu and Goud [16].

It is noticed that the research studies mentioned above are confined to no-slip conditions at the boundary wall. However, it may not be appropriate to ignore the slip factor when the fluid flows over a stretching surface. Claude-Louis Navier was the first to describe the significance of velocity slip in the flow field in 1823. Velocity slip impact on nanofluid flow has found various applications in polishing artificial heart valves, biological fluids, lubrication, and other engineering and manufacturing processes. Ensuring this, Basir et al. [17] elaborated on multiple slips, Schmidt number and Peclet number aspects of nanofluid flow past a stretching cylinder. Velocity slip and inclined magnetic field effects on nanofluid flow towards a stretching cylinder in the presence of curvature slip were analyzed by Degavath and Kishan [18]. Multiple slips, chemical reactions and magnetic dipole influences on nanofluid flow along a stretching cylinder were numerically solved by Alshomrani and Ramzan [19]. Hamid et al. [20] analyzed multiple slips and variable thermal conductivity impacts on magnetite nanofluid flow past an elongating surface considering first-order chemical reaction. Tlili et al. [21] deliberated multiple slips and magnetic field combined aspects on hybrid nanofluid flow generated by a stretching surface. Inclined magnetic field and velocity slip impacts on hybrid nanofluid flow towards a stretching cylinder with thermal slip were presented by Abbas et al. [22].

In a viscous fluid, viscous dissipation is the rate at which kinetic energy is transformed into thermal energy per unit mass. Viscous and Ohmic dissipations are essential for thermal transport phenomena when fluid flows past a stretching cylindrical body. These effects play a significant role during the heat transportation of fluid overheated surfaces. Based on such massive occurrences, viscous and Ohmic dissipations effect on nanofluid flow past a stretching cylinder with magnetic field effect was canvassed by Hussain et al. [23]. Ghadikolaei et al. [24] presented viscous dissipation influence on Second-grade nanofluid flow generated by an elongating surface. Viscous and Joule dissipation impacts on magnetic hybrid nanofluid flow past a stretching cylinder were numerically solved by Maskeen et al. [25]. Shah et al. [26] presented Ohmic and viscous dissipation influences on EMHD nanofluid flow over a porous plate considering the Hall effect. Viscous and Joule dissipation effects on magneto-hybrid nanofluid flow along a stretching sheet with the Cattaneo–Christov heat flux model was elaborated by Tassaddiq [27].

The presence of a heat source/generation typically plays a vital role in boundary layer flows with heat transfer because the heat source determines the direction of the temperature inside the boundary layer and the fabrication and quality of the final product are controlled by this factor. Semi-conductor wafers, nuclear reactors, combustion modeling, electronic chips and endothermic chemical reaction are some practical applications of the presence of heat source in the flow field (see, Refs. [28,29]). In light of this significance, the simultaneous impacts of heat generation and Joule dissipation on magneto-nanofluid flow induced by a stretching cylinder with viscous dissipation and velocity slip were illustrated by Mishra et al. [30]. Hashim et al. [31] deliberated heat source, magnetic field and variable thermal conductivity influences on mixed convective Williamson nanofluid flow past a radially stretched sheet. Time-dependent magneto-nanofluid flow induced by a cylinder taking heat source, activation energy, zero mass flux and binary chemical reaction into account was examined by Hamid et al. [32]. Later on, Mishra and Kumar [33] illustrated heat source impact on magnetic nanofluid flow past a stretching cylinder considering multiple slips and viscous-Ohmic dissipation. Mabood et al. [34] addressed heat generation and inclined magnetic field effects on nanofluid flow past a permeable stretching cylinder in the presence of viscous dissipation, thermal buoyancy force, Ohmic dissipation and Newtonian heating. Heat source and melting effect on magnetic nanofluid flow towards a stretching cylinder under porous medium was illustrated by Singh et al. [35]. Heat generation and multiple slips impacts on hybrid nanofluid flow along a porous stretching sheet were studied by Wahid et al. [36].

Thermal radiation is a process in which energy is released in the form of electromagnetic waves, which move at the speed of light and no medium is required for its propagation. Infrared rays, visible light, and ultraviolet rays are all types of thermal radiation. Light coming from the sun, heating components on a stove, fire and radiators are some examples of thermal radiation. Thermal radiation impact on boundary layer fluid flow has observed profound applications in engineering and industrial fields. Some of these are found in furnace design, gas-cooled nuclear reactors, polymer processing, and space technology like missiles, aerodynamics rockets, propulsion systems, and spacecraft, which operate at high temperatures (see, Refs. [37–40]). Such applications lead Acharya et al. [41] to describe thermal radiation and non-uniform heat source aspects for unsteady magnetite nanofluid flow generated by a stretching cylinder in the presence of velocity slip. Thermal radiation and thermal buoyancy force effects on Cu-H₂O nanofluid flow past a stretching cylinder in the presence of heat generation, viscous dissipation and multiple slips were discussed by Pandey and Kumar [42]. Thermal radiation aspect on magnetic nanofluid flow past a stretching cylinder under porous medium taking viscous dissipation and Ohmic heating into account was investigated by Zeeshan et al. [43]. Ghadikolaei et al. [44] illustrated thermal radiation and nanoparticles shape effects on magneto hybrid nanofluid flow generated by a rotating cone taking thermal buoyancy force and heat generation into account. The aspects of thermal radiation and viscous-Ohmic dissipation on MHD dusty micropolar nanofluid flow along an elongating sheet under a porous medium were explored by Ghadikolaei et al. [45]. Vinita and Poply [46] examined thermal radiation and velocity slip influences on stagnation point flow of nanofluid past a stretching cylinder considering heat generation. The sway of thermal radiation and temperature-dependent thermal conductivity on hybrid base fluid-based magnetite hybrid nanofluid flow towards an elongating surface with mixed convection, rotation and suction/injection was

deliberated by Ghadikolaei et al. [47]. Thermal radiation and mixed convection combined aspects on time-dependent magnetic nanofluid flow generated by a stretching cylinder were reported by Hamid et al. [48]. Vinita et al. [49] analyzed the combined effects of thermal radiation and multiple slips on magneto-nanofluid flow towards a stretching cylinder, taking viscous and Joule dissipations into account.

The heat transfer rate at the surface is described by the convective heating condition, which directly relates to the local temperature difference in ambient conditions. Furthermore, the thermal conductivity and nanofluid's temperature are increased by convective heating at the boundary surface. As a result, the convective heating condition is more effective at the boundary surface than the constant wall temperature condition. Hence, it has noticed widespread use in thermal energy storage, gas turbines, nuclear turbines, die forging, etc. Khan et al. [50] addressed convective heating condition impact on magneto nanofluid flow induced by a stretching cylinder with mixed convection. Convective heating boundary condition and velocity slip influences on nanofluid flow past a permeable stretching cylinder were studied by Bakar et al. [51]. Convective heating and velocity slip impacts on magnetite nanofluid flow past a thermally radiated stretched surface within a porous medium considering variable thermal conductivity and viscous dissipation were examined by Ghadikolaei and Gholinia [52]. Convective heating condition and velocity slip effects on 3-dimensional hybrid nanofluid flow towards a permeable stretching surface were investigated by Khashi'ie et al. [53]. Ghadikolaei and Gholinia [54] presented sway of convective heating and velocity slip on hybrid base fluid-based nanofluid flow along a stretching surface taking viscous dissipation, free convection and thermal radiation into account. Convective heating, viscous dissipation and Joule heating influences on MHD stagnation point flow of a hybrid nanofluid past a stretching sheet were discussed by Anuar et al. [55]. Hussain et al. [56] illustrated convective condition and rotation aspects on three-dimensional hybrid nanofluid flow induced by a permeable stretching sheet. Effects of convective heating and zero mass flux conditions at the boundary on unsteady nanoliquid flow along a wedge shape geometry with a magnetic field was given by Hamid [57].

After going through the above-mentioned good literature, it is observed that no attention has been given yet to the unsteady stagnation flow of a hybrid nanofluid past a stretching cylinder. So, in the present analysis, our primary focus is to examine the unsteady stagnation point flow of hybrid nanofluid (Cu-Al₂O₃/H₂O) past a convectively heated stretching cylinder. Further, the influences of velocity slip, inclined magnetic field, Joule dissipation, thermal radiation, viscous dissipation and heat generation are also incorporated into this study. This study may find its importance in several engineering and manufacturing processes and devices, viz. geothermal energy extractions, turbines, thermal energy storage, nuclear reactors, forging and levitation, combustion modeling and many more. With the help of appropriate similarity transformations, the governing dimensional mathematical equations are converted to non-dimensional form and solved numerically using 5th order Runge–Kutta–Fehlberg method-based shooting technique. Figures and numerical data presented in tabular form are used to describe the physical aspects of the behavior of different controlling parameters on the flow and thermal fields. Multiple regression analysis is also performed to estimate the local surface drag coefficient and local Nusselt number.

2. Mathematical formulation

2.1. Flow assumptions and physical configuration

Consider the unsteady and free-convective stagnation point flow of an incompressible, viscous hybrid nanofluid (Cu-Al₂O₃/H₂O) past a continuously moving and convectively heated stretching cylinder under the influence of Lorentz force with velocity slip at the solid surface. The presence of thermal radiation, heat generation, viscous and Ohmic dissipations are also incorporated into the analysis. The coordinate system is chosen in such a way that the x -axis is measured along the cylinder and the r -axis is measured along the radial direction of the cylinder. Let R be the radius of the stretching cylinder. The stretching velocity of the cylindrical sheet is $u_{\text{wall}} = \frac{ax}{1-\lambda t}$ and the free-stream velocity of the hybrid nanofluid is $u_{\infty} = \frac{bx}{1-\lambda t}$, where a , b and λ are positive constants while $\lambda t < 1$ with dimension of λ as (time)⁻¹. A variable magnetic field of intensity $B_0 = \frac{B_1}{\sqrt{1-\lambda t}}$ is acted in the flow-field in an inclined direction making an angle ϕ with the vertical. A hot fluid of temperature T_{wall} with variable convective heat transfer coefficient $h_1 = \frac{h_2}{\sqrt{1-\lambda t}}$ is flowing below the stretching cylinder. The space and time-dependent surface temperature of the stretching cylinder is $T_{\text{wall}} = T_{\infty} + \frac{T_0 x}{l(1-\lambda t)}$ whereas the constant temperature of the hybrid nanofluid outside the boundary layer is T_{∞} . Also, compare to the applied magnetic field, the impact of induced magnetic field is neglected on the basis that the magnetic Reynolds number is very small. A schematic diagram describing the fluid flow problem under consideration is presented in Fig. 1.

2.2. Model equations

Based on the assumptions made in the previous subsection and following the articles [22,34,41], the governing boundary layer equations for the present problem can be written as

Continuity equation:

$$\frac{\partial(ru)}{\partial x} + \frac{\partial(rv)}{\partial r} = 0, \quad (1)$$

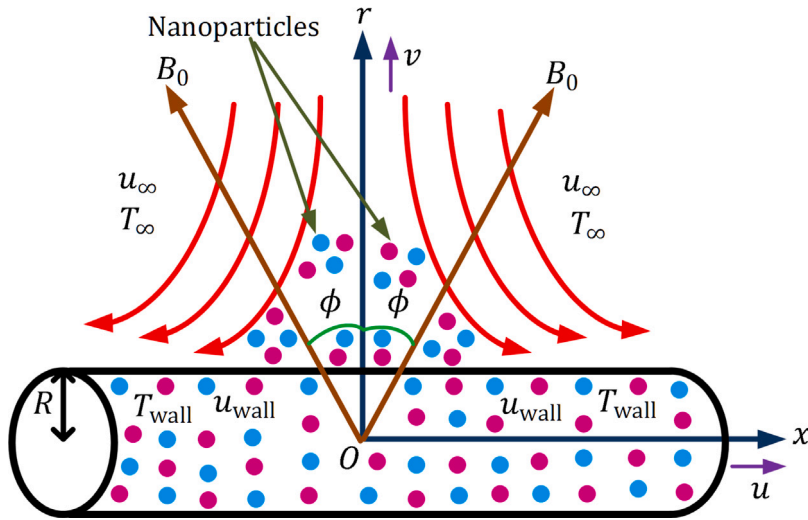


Fig. 1. Schematic diagram of the fluid flow problem.

Momentum equation:

$$\frac{\partial u}{\partial t} + u \frac{\partial u}{\partial x} + v \frac{\partial u}{\partial r} = \frac{\partial u_{\infty}}{\partial t} + u_{\infty} \frac{\partial u_{\infty}}{\partial x} + \frac{\mu_{\text{hnf}}}{\rho_{\text{hnf}}} \left(\frac{\partial^2 u}{\partial r^2} + \frac{1}{r} \frac{\partial u}{\partial r} \right) - \frac{\sigma_{\text{hnf}} B_0^2}{\rho_{\text{hnf}}} (u - u_{\infty}) \sin^2 \phi + g \frac{(\rho\beta)_{\text{hnf}}}{\rho_{\text{hnf}}} (T - T_{\infty}), \quad (2)$$

Energy equation:

$$\begin{aligned} \frac{\partial T}{\partial t} + u \frac{\partial T}{\partial x} + v \frac{\partial T}{\partial r} = & \frac{k_{\text{hnf}}}{(\rho c_p)_{\text{hnf}}} \left(\frac{\partial^2 T}{\partial r^2} + \frac{1}{r} \frac{\partial T}{\partial r} \right) - \frac{1}{(\rho c_p)_{\text{hnf}}} \frac{\partial q_r}{\partial r} + \frac{\sigma_{\text{hnf}} B_0^2}{(\rho c_p)_{\text{hnf}}} (u - u_{\infty})^2 \sin^2 \phi + \frac{\mu_{\text{hnf}}}{(\rho c_p)_{\text{hnf}}} \left(\frac{\partial u}{\partial r} \right)^2 \\ & + \frac{Q_0}{(\rho c_p)_{\text{hnf}}} (T - T_{\infty}). \end{aligned} \quad (3)$$

The related boundary conditions are prescribed as follows:

$$\text{When } t \leq 0 : u = 0, \quad v = 0, \quad T = T_{\infty} \quad \text{for all } r \geq 0,$$

$$\text{When } t > 0 : u = u_{\text{wall}} + N_1 \frac{\mu_{\text{hnf}}}{\rho_{\text{hnf}}} \frac{\partial u}{\partial r}, \quad v = 0, \quad -k_{\text{hnf}} \frac{\partial T}{\partial r} = h_1 (T_{\text{wall}} - T) \quad \text{for } r = R \quad (4)$$

$$u \rightarrow u_{\infty}, \quad T \rightarrow T_{\infty} \quad \text{for } r \rightarrow \infty.$$

According to Rosseland's radiative flux model for an optically thick medium, the radiative heat flux q_r is described as (see, Ref. [41])

$$q_r = -\frac{4\sigma^*}{3k^*} \frac{\partial T^4}{\partial r}. \quad (5)$$

Considering small temperature difference between free-stream and the fluid within the boundary layer, T^4 is expanded in Taylor's series about T_{∞} . After retaining the linear terms only, we obtain

$$T^4 \cong 4T_{\infty}^3 T - 3T_{\infty}^4. \quad (6)$$

2.3. Similarity transformation and non-dimensional equations

The following similarity transformation is introduced in order to simplify the problem to a similar form (see, Ref. [41]):

$$\psi = \left(\frac{av_{\text{bf}}}{1 - \lambda t} \right)^{1/2} x R f(\eta), \quad \eta = \frac{r^2 - R^2}{2R} \left\{ \frac{a}{v_{\text{bf}}(1 - \lambda t)} \right\}^{1/2}, \quad \theta(\eta) = \frac{T - T_{\infty}}{T_{\text{wall}} - T_{\infty}}. \quad (7)$$

Making use of Eq. (6) along with above similarity transformation in Eqs. (2) and (3), we obtain the following dimensionless nonlinear coupled ODEs:

$$\alpha_1 (1 + 2\eta\beta_1) f''' + (2\beta_1\alpha_1 + \alpha_2 f) f'' - \alpha_2 f'^2 - A\alpha_2 \left(f' + \frac{\eta}{2} f'' \right) + A\alpha_2 \lambda_1 + \alpha_2 \lambda_1^2 - \alpha_3 \alpha_4 M (f' - \lambda_1) \sin^2 \phi + \alpha_5 Gr\theta = 0, \tag{8}$$

$$\left(\alpha_6 \alpha_7 + N \right) \left(1 + 2\eta\beta_1 \right) \theta'' - A\alpha_8 Pr \left(\theta + \frac{\eta}{2} \theta' \right) - \alpha_8 Pr (f'\theta - f\theta') + \beta_1 \theta' (2\alpha_6 \alpha_7 + N) + QPr\theta + \alpha_3 \alpha_4 PrEcM (f' - \lambda_1)^2 \sin^2 \phi + \alpha_1 PrEc (1 + 2\eta\beta_1) f''^2 = 0. \tag{9}$$

The related boundary conditions, in dimensionless form, are written as

$$f(0) = 0, \quad f'(0) = 1 + \frac{\alpha_1}{\alpha_2} \delta f''(0), \quad \theta'(0) = -\frac{\gamma}{\alpha_6 \alpha_7} \{1 - \theta(0)\}, \quad f'(\infty) \rightarrow \lambda_1, \quad \theta(\infty) \rightarrow 0. \tag{10}$$

The mathematical expressions for the dimensionless parameters associated with Eqs. (8)–(10) are mentioned below:

$$A = \frac{\lambda}{a}, \quad \alpha_1 = \frac{\mu_{hnf}}{\mu_{bf}}, \quad \alpha_2 = \frac{\rho_{hnf}}{\rho_{bf}}, \quad \alpha_3 = \frac{\sigma_{hnf}}{\sigma_{nf}}, \quad \alpha_4 = \frac{\sigma_{nf}}{\sigma_{bf}}, \quad \alpha_5 = \frac{(\rho\beta)_{hnf}}{(\rho\beta)_{bf}}, \quad \alpha_6 = \frac{k_{hnf}}{k_{nf}}, \quad \alpha_7 = \frac{k_{nf}}{k_{bf}},$$

$$\alpha_8 = \frac{(\rho c_p)_{hnf}}{(\rho c_p)_{bf}}, \quad \beta_1 = \frac{1}{R} \sqrt{\frac{v_{bf}(1-\lambda t)}{a}}, \quad M = \frac{\sigma_{bf} B_1^2}{a \rho_{bf}}, \quad Gr = \frac{g(\rho\beta)_{bf} T_0 (1-\lambda t)}{l a^2 \rho_{bf}}, \quad Pr = \frac{v_{bf} (\rho c_p)_{bf}}{k_{bf}},$$

$$Q = \frac{Q_1}{a (\rho c_p)_{bf}}, \quad N = \frac{16\sigma^* T_\infty^3}{3k_{bf} k^*}, \quad Ec = \frac{u_{wall}^2}{(c_p)_{bf} (T_{wall} - T_\infty)}, \quad \delta = N_2 \sqrt{a v_{bf}}, \quad \gamma = \frac{h_2}{k_{bf}} \sqrt{\frac{v_{bf}}{a}}, \quad \lambda_1 = \frac{b}{a}.$$

2.4. Physical quantities from engineering perspective

From engineering point of view, the physical quantities of interest for the fluid flow with heat transfer along a solid surface are the skin-friction coefficient and the Nusselt number. These quantities are defined below (see, Refs. [22,41]):

$$C_{f_r} = \frac{2\tau_{wall}}{\rho_{bf} u_{wall}^2}, \tag{11}$$

where $\tau_{wall} = \mu_{hnf} \frac{\partial u}{\partial r} \Big|_{r=R}$ measures the shear stress at the surface of the stretching cylinder.

$$Nu_r = \frac{xq_{wall}}{k_{bf} (T_{wall} - T_\infty)}, \tag{12}$$

where $q_{wall} = -\left(k_{hnf} + \frac{16\sigma^* T_\infty^3}{3k^*} \right) \frac{\partial T}{\partial r} \Big|_{r=R}$ signifies the rate of heat transfer at the surface of the stretching cylinder.

The skin-friction coefficient and the Nusselt number, in dimensionless form, can be expressed as

$$C_{f_r} Re_x^{1/2} = 2\alpha_1 f''(0), \tag{13}$$

$$Nu_r Re_x^{-1/2} = -(\alpha_6 \alpha_7 + N) \theta'(0). \tag{14}$$

Here, $Re_x = \frac{xu_{wall}}{\nu_f}$ represents the local Reynolds number.

2.5. Thermo-physical relations

The authors of this paper attempted to use a novel approach to alter the manner of heat transmission in liquids that scientists had lately studied. The authors of this paper claim to have used hybrid nanoparticles in combination with several types of nanoparticles and a hybrid base liquid. The current method should be a great way to improve the heat transmission process in liquids. The relations among the respective thermo-physical properties like viscosity, density, heat capacity, electrical and thermal conductivities etc. of nanofluid, hybrid nanofluid and normal base fluid are prescribed in Table 1. To get the thermo-physical relation for the thermal conductivity, we have followed the Xue model (see, Ref. [22]). Further, the numerical values of the thermo-physical quantities of nanoparticles (Al₂O₃ and Cu) and base fluid (H₂O) are presented in Table 2.

3. Numerical technique

3.1. Applied numerical technique

It is noticed that Eqs. (8) and (9) together constitute a highly nonlinear system. So, in order to get numerical solutions to such nonlinear system subject to the endpoint constraints mentioned in (10), the well-known shooting technique based on Runge–Kutta–Fehlberg method of 5th order (see, Ref. [33]) is employed. For this reason, new set of variables $\Omega_1, \Omega_2, \Omega_3, \Omega_4, \Omega_5$ are chosen in such a way that $(\Omega_1, \Omega_2, \Omega_3, \Omega_4, \Omega_5)^{T*} = (f, f', f'', \theta, \theta')^{T*}$, T^* being the transpose. After applying above noted new variables in

Table 1
Thermo-physical relations for nanofluid and hybrid nanofluid (Following, Refs. [22,55] and [58]).

Fluid type	Thermo-physical relations
Nanofluid	$\mu_{nf} = \frac{\mu_f}{(1 - \Phi_1)^{2.5}}$ $\rho_{nf} = \Phi_1 \rho_{n_1} + \rho_f (1 - \Phi_1)$ $(\rho c_p)_{nf} = \Phi_1 (\rho c_p)_{n_1} + (\rho c_p)_f (1 - \Phi_1)$ $k_{nf} = \frac{1 - \Phi_1 + 2\Phi_1 \left(\frac{k_{n_1}}{k_{n_1} - k_f} \right) \ln \left(\frac{k_{n_1} + k_f}{2k_f} \right)}{1 - \Phi_1 + 2\Phi_1 \left(\frac{k_f}{k_{n_1} - k_f} \right) \ln \left(\frac{k_{n_1} + k_f}{2k_f} \right)} \times k_f$ $(\rho\beta)_{nf} = \Phi_1 (\rho\beta)_{n_1} + (\rho\beta)_f (1 - \Phi_1)$ $\sigma_{nf} = \frac{\sigma_{n_1} (1 + 2\Phi_1) + 2\sigma_f (1 - \Phi_1)}{\sigma_{n_1} (1 - \Phi_1) + \sigma_f (2 + \Phi_1)} \times \sigma_f$
Hybrid nanofluid	$\mu_{hnf} = \frac{\mu_f}{(1 - \Phi_1)^{2.5} (1 - \Phi_2)^{2.5}}$ $\rho_{hnf} = \Phi_2 \rho_{n_2} + \{ \Phi_1 \rho_{n_1} + \rho_f (1 - \Phi_1) \} (1 - \Phi_2)$ $(\rho c_p)_{hnf} = \Phi_2 (\rho c_p)_{n_2} + \{ \Phi_1 (\rho c_p)_{n_1} + (\rho c_p)_f (1 - \Phi_1) \} (1 - \Phi_2)$ $k_{hnf} = \frac{1 - \Phi_2 + 2\Phi_2 \left(\frac{k_{n_2}}{k_{n_2} - k_{nf}} \right) \ln \left(\frac{k_{n_2} + k_{nf}}{2k_{nf}} \right)}{1 - \Phi_2 + 2\Phi_2 \left(\frac{k_{nf}}{k_{n_2} - k_{nf}} \right) \ln \left(\frac{k_{n_2} + k_{nf}}{2k_{nf}} \right)} \times k_{nf}$ $(\rho\beta)_{hnf} = \Phi_2 (\rho\beta)_{n_2} + \{ \Phi_1 (\rho\beta)_{n_1} + (\rho\beta)_f (1 - \Phi_1) \} (1 - \Phi_2)$ $\sigma_{hnf} = \frac{\sigma_{n_2} (1 + 2\Phi_2) + 2\sigma_{nf} (1 - \Phi_2)}{\sigma_{n_2} (1 - \Phi_2) + \sigma_{nf} (2 + \Phi_2)} \times \sigma_{nf}$

Table 2
Thermo-physical properties of Cu, Al₂O₃ and H₂O (Following, Refs. [36] and [55]).

Physical properties	H ₂ O	Al ₂ O ₃	Cu
ρ (kg/m ³)	997.1	3970	8933
σ (Ω^{-1} m ⁻¹)	0.05	1×10^{-10}	5.96×10^7
$\beta \times 10^{-5}$ (1/K)	21	0.85	1.67
k (W/m K)	0.613	40	400
c_p (J/kg K)	4179	765	385

Eqs. (8) and (9) together with boundary conditions (10), the resulting set of equations and the boundary constraints are represented as

$$\begin{pmatrix} \Omega'_1 \\ \Omega'_2 \\ \Omega'_3 \\ \Omega'_4 \\ \Omega'_5 \end{pmatrix} = \begin{pmatrix} \Omega_2 \\ \Omega_3 \\ \frac{\alpha_2 \Omega_2^2 + A\alpha_2 (\Omega_2 + \frac{\eta}{2} \Omega_3) - (2\beta_1 \alpha_1 + \alpha_2 \Omega_1) \Omega_3 - A\alpha_2 \lambda_1 - \alpha_2 \lambda_1^2 + \alpha_3 \alpha_4 M (\Omega_2 - \lambda_1) \sin^2 \phi - \alpha_5 Gr \Omega_4}{\alpha_1 (1 + 2\eta\beta_1)} \\ \Omega_5 \\ \frac{A\alpha_8 Pr (\Omega_4 + \frac{\eta}{2} \Omega_5) + \alpha_8 Pr (\Omega_2 \Omega_4 - \Omega_1 \Omega_5) - (2\alpha_6 \alpha_7 + N) \beta_1 \Omega_5 - Q Pr \Omega_4 - \alpha_3 \alpha_4 Pr Ec M (\Omega_2 - \lambda_1)^2 \sin^2 \phi - \alpha_1 Pr Ec (1 + 2\eta\beta_1) \Omega_3^2}{(\alpha_6 \alpha_7 + N) (1 + 2\eta\beta_1)} \end{pmatrix}$$

The transformed boundary conditions are written in the following form

$$\Omega_1(0) = 0, \Omega_2(0) = 1 + \frac{\alpha_1}{\alpha_2} \delta \Omega_3(0), \Omega_5 = -\frac{\gamma}{\alpha_6 \alpha_7} \{ 1 - \Omega_4(0) \}, \Omega_2(\infty) \rightarrow \lambda_1, \Omega_4(\infty) \rightarrow 0.$$

The formula of Runge–Kutta–Fehlberg technique for solving the initial value problem

$$\frac{dY}{dX} = F(X, Y), \quad Y(X_0) = Y_0$$

is given by

$$Y_{i+1} = Y_i + \frac{16}{135} \Sigma_1 + \frac{6656}{12825} \Sigma_3 + \frac{28561}{56430} \Sigma_4 - \frac{9}{50} \Sigma_5 + \frac{2}{55} \Sigma_6, \quad i = 0, 1, 2, \dots$$

Table 3
Validation of the obtained numerical values of $-f''(0)$ for different values of δ .

δ	Present study	Sahoo and Do [59]	Noghrehabadi et al. [60]
0.0	1.000008	1.001154	1.000000
0.5	0.591211	0.589195	0.591195
1.0	0.430180	0.428450	0.430160
2.0	0.284005	0.282893	0.283980
3.0	0.214083	0.213314	0.214055
5.0	0.144871	0.144430	0.144841

Table 4
Test for stability of the numerical method and grid independence of the obtained results.

η	$f'(\eta)$			$\theta(\eta)$		
	$h = 0.1$	$h = 0.01$	$h = 0.001$	$h = 0.1$	$h = 0.01$	$h = 0.001$
0.0	0.6450687854	0.6450688322	0.6450688326	0.0423252615	0.0423253040	0.0423253042
1.0	0.4322090783	0.4322090550	0.4322090573	0.0098588289	0.0098588664	0.0098588665
2.0	0.4068325138	0.4068322988	0.4068323065	0.0026334664	0.0026335128	0.0026335131
3.0	0.4018157105	0.4018150857	0.4018151068	0.0007965925	0.0007966685	0.0007966692
4.0	0.4004922285	0.4004906925	0.4004907438	0.0002238167	0.0002239408	0.0002239419
5.0	0.4000000000	0.4000000000	0.4000000000	0.0000000000	0.0000000000	0.0000000000

where

$$\begin{aligned} \Sigma_1 &= h_1 f(X_i, Y_i), \\ \Sigma_2 &= h_1 f\left(X_i + \frac{1}{4}h_1, Y_i + \frac{1}{4}\Sigma_1\right), \\ \Sigma_3 &= h_1 f\left(X_i + \frac{3}{8}h_1, Y_i + \frac{3}{32}\Sigma_1 + \frac{9}{32}\Sigma_2\right), \\ \Sigma_4 &= h_1 f\left(X_i + \frac{12}{13}h_1, Y_i + \frac{1932}{2197}\Sigma_1 - \frac{7200}{2197}\Sigma_2 + \frac{7296}{2197}\Sigma_3\right), \\ \Sigma_5 &= h_1 f\left(X_i + h_1, Y_i + \frac{439}{216}\Sigma_1 - 8\Sigma_2 + \frac{3680}{513}\Sigma_3 - \frac{845}{4104}\Sigma_4\right), \\ \Sigma_6 &= h_1 f\left(X_i + \frac{1}{2}h_1, Y_i - \frac{8}{27}\Sigma_1 + 2\Sigma_2 - \frac{3544}{2565}\Sigma_3 + \frac{1859}{4104}\Sigma_4 - \frac{11}{40}\Sigma_5\right). \end{aligned}$$

To implement the solution technique, suitable guess values are assumed for the unavailable initial conditions. These guess values are modified using the secant iteration until the appropriate initial conditions are recovered. The convergence tolerance and the step size are taken as 10^{-6} and 0.01 respectively. For the far-field boundary conditions (i.e., as $\eta \rightarrow \infty$), an appropriate finite value for η , say $\eta_\infty = 5$ is considered. The graphical illustrations confirm that all the conditions outside the boundary layer are satisfied with this value of η .

3.2. Validation and accuracy

As a test of the correctness and accuracy of the obtained numerical results, we have calculated the values of $-f''(0)$ for altered values of the curvature parameter δ for a specific case of the present study, i.e., when $A = \beta_1 = \lambda_1 = \Phi_1 = \Phi_2 = Gr = 0$ and $\phi = \pi/2$. The computed values are compared with the results reported earlier by Sahoo and Do [59] and Noghrehabadi et al. [60]. The comparison is nicely depicted in Table 3. For such limiting case of the study, a fantastic agreement among the results is noticed from the table. This clearly indicate that our obtained results are correct and reliable. Moreover, it validates the correctness of the written computer code for the used numerical technique.

3.3. Stability and convergence

Table 4 demonstrates the grid invariance test for the velocity and temperature of the hybrid nanofluid. The table justifies the stability of the applied numerical technique for the current analysis. It is observed from the table that when the number of elements in the same domain is increased and the step size is reduced, the results remain almost unchanged. This implies that the obtained results are grid independent and hence the applied numerical method is quite stable and convergent.

4. Results and discussion

The ongoing section deals with the sway of prominent flow parameters, viz. unsteadiness parameter A , velocity ratio parameter λ_1 , magnetic parameter M , inclination parameter ϕ , velocity slip parameter δ , thermal Grashof number Gr , Biot number γ , Eckert number Ec , thermal radiation parameter N and heat generation parameter Q on the velocity as well as temperature fields. The outcomes are explained with the help of graphical profiles as depicted in Figs. 2–15. Furthermore, the impact of the aforementioned

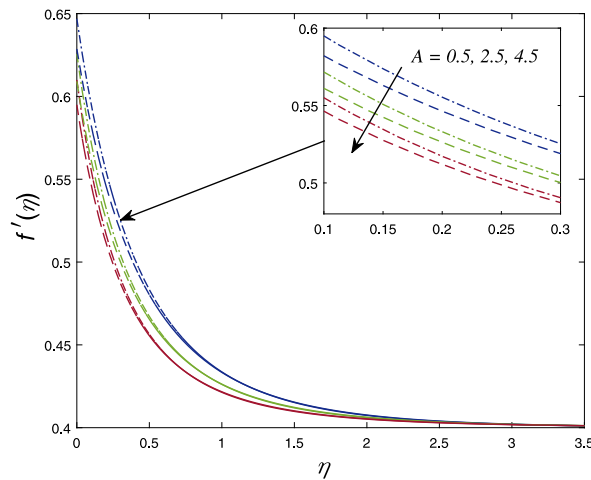


Fig. 2. Depiction of $f'(\eta)$ for altered values of A .

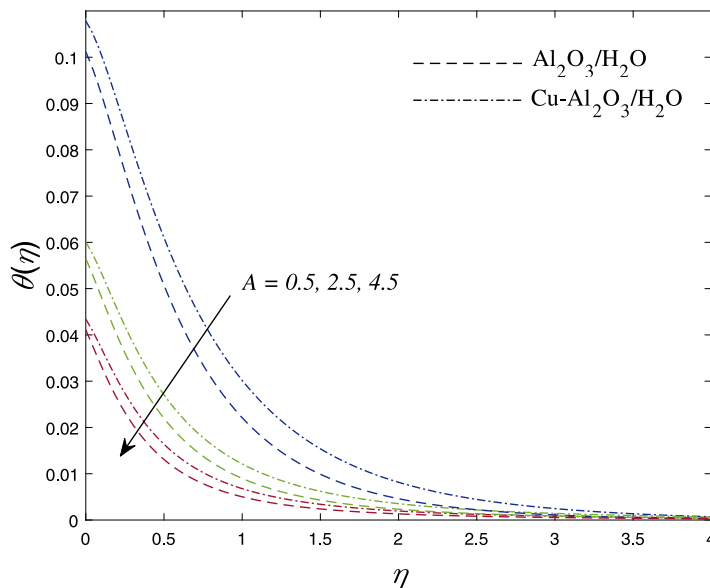


Fig. 3. Depiction of $\theta(\eta)$ for altered values of A .

quantities on local surface drag coefficient and heat transfer rate at the surface are also explained and the numerical results are presented in tabular form. The entire computation and the demonstration have been achieved by fixing the parameters' default values as $A = 0.5$, $\lambda_1 = 0.4$, $M = 5.0$, $\phi = \pi/3$, $\delta = 0.7$, $Gr = 0.5$, $\gamma = 0.1$, $Ec = 0.5$, $N = 0.2$, $Q = 0.1$, $Pr = 6.2$, $\beta_1 = 0.5$, $\Phi_1 = \Phi_2 = 0.05$. The parameter values are chosen by consulting some relevant good research works existing in the literature.

Figs. 2 and 3 are plotted to visualize the behavior of the velocity and temperature profiles in the cases of nanofluid and hybrid nanofluid against the variations in unsteadiness parameter A . The figures show that when the value of A rises, the velocity and temperature profiles decrease in both cases. Physically, as unsteadiness enhances, the sheet loses more heat, due to which temperature falls. To elucidate the effect of velocity ratio parameter λ_1 on velocity and temperature distributions in both the cases (nanofluid and hybrid nanofluid), Figs. 4 and 5 are sketched. The sketched traces clearly reveal that for intensifying values of λ_1 , the velocity profile is uplifted in both cases. However, there is a gradual reduction in the nanofluid and hybrid nanofluid temperature profiles with respect to λ_1 . From a physical point of view, for rising values of velocity ratio parameter impact of free stream velocity of nanofluid is more compared to the nanofluid velocity at the sheet's surface due to this velocity profile is enhanced. Figs. 6 and 7 explore the impact of magnetic parameter M on velocity as well as temperature profiles w.r.t. nanofluid and hybrid nanofluid respectively. In both the cases for increasing values of M , we noticed a decreasing trend in the velocity profile and an increasing trend in the temperature profile. A resistive force named Lorentz force is generated when a magnetic field is employed in an electrically conducting liquid. Due to this retarding force $f'(\eta)$ is lowered and $\theta(\eta)$ is escalated for steadily amplifying values of M . The velocity

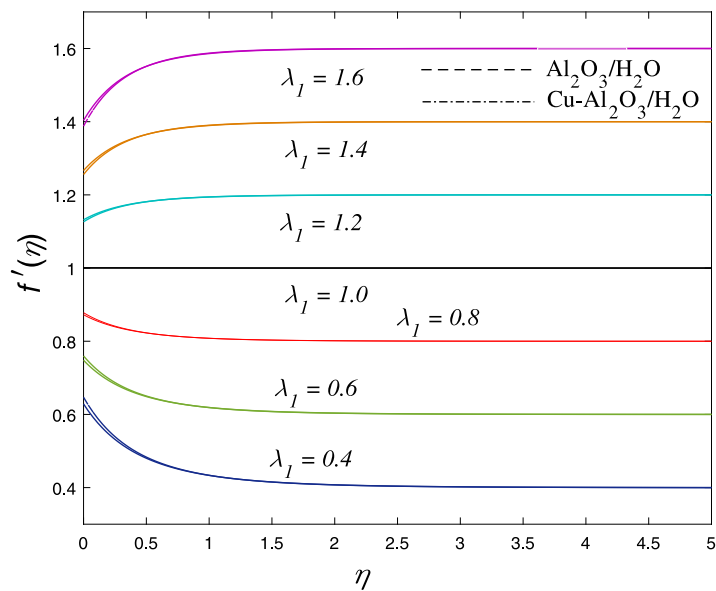


Fig. 4. Depiction of $f'(\eta)$ for altered values of λ_1 .

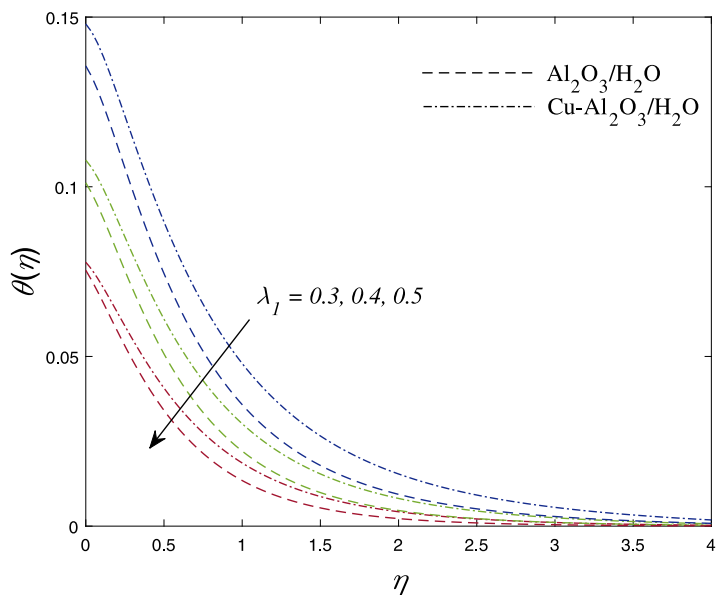


Fig. 5. Depiction of $\theta(\eta)$ for altered values of λ_1 .

and temperature distributions under the action of inclined angle parameter ϕ are plotted in Figs. 8 and 9 for nanofluid as well as hybrid nanofluid. It is clearly visible from figures that for upsurging values of ϕ , $f'(\eta)$ is worsened and $\theta(\eta)$ is intensified for both the cases. Viscosity dissipation boosts thermal improvement near the surface. Due to this reason $f'(\eta)$ is diminished and $\theta(\eta)$ is enhanced for boosting values of ϕ . The sway of the first nanoparticles volume fraction parameter Φ_1 on velocity and temperature profiles of nanofluid as well as hybrid nanofluid is presented in Figs. 10 and 11. From Fig. 10 it is observed that in both the cases velocity profile is diminished w.r.t. Φ_1 . This is because the flow slows down due to the addition of other nanoparticles to the flow. The temperature profiles of nanofluid and hybrid nanofluid are enhanced for gradually boosting values of Φ_1 , which is seen from Fig. 11. The nanoparticles physically dissipate energy in the form of heat. Adding additional nanoparticles simultaneously extends more heat, enhancing the temperature of both nanofluid and hybrid nanofluid. The velocity profile $f'(\eta)$ for altered values of velocity slip parameter δ is shown in Fig. 12 w.r.t. nanofluid and hybrid nanofluid. We observe that in both cases, the flow profile is declined for upsurging values of δ . It is because partial slip mainly slows down fluid motion, confirming a decrease in the net flow of fluid molecules. As a consequence of less molecular acceleration, the velocity profile is reduced. Fig. 13 is drawn to examine

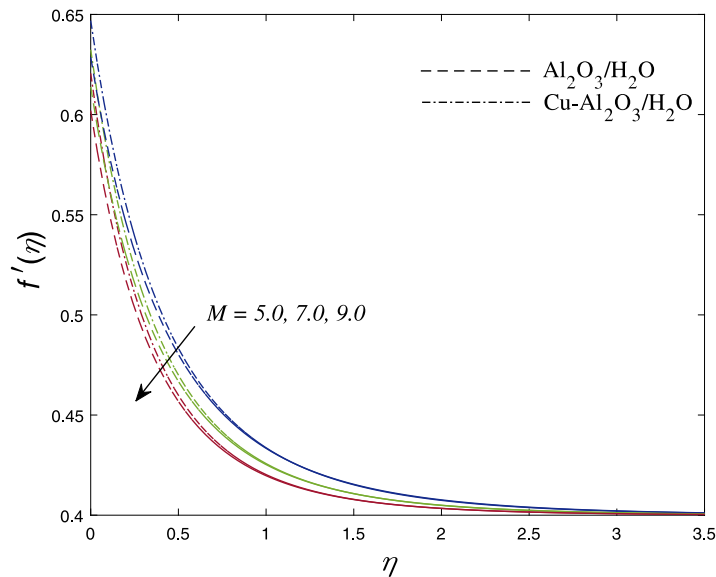


Fig. 6. Depiction of $f'(\eta)$ for altered values of M .

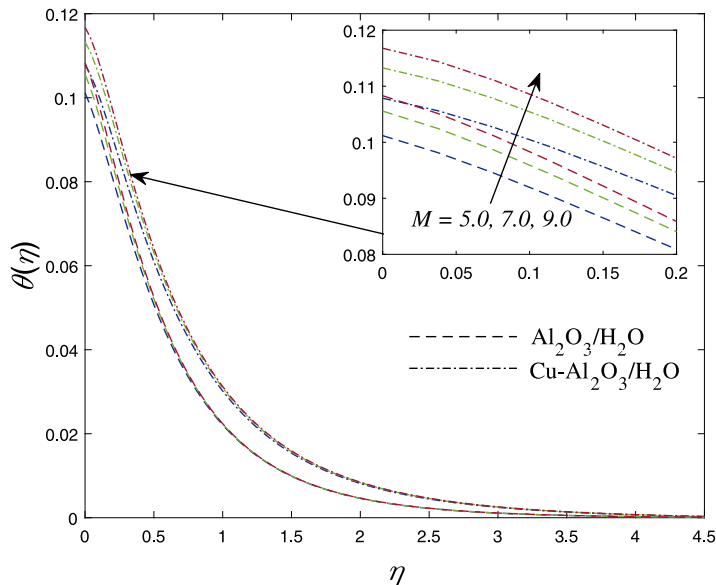


Fig. 7. Depiction of $\theta(\eta)$ for altered values of M .

the impact of thermal buoyancy parameter Gr on the velocity profile for nanofluid and hybrid nanofluid. It is concluded that the velocity profile is enhanced for growing values of Gr everywhere in the boundary layer region for both cases. In view of physics, if the buoyancy parameter value increases, the effect viscous forces in the fluid decreases and the buoyancy force has the tendency to induce the fluid motion. As a result, the fluid velocity is increased. The graphical illustration for temperature variation with respect to Biot number γ is displayed in Fig. 14 for nanofluid and hybrid nanofluid. The pictured result shows that the increment in Biot number enhances the temperature profile for nanofluid as well as hybrid nanofluid. Physically, the thermal Biot number directly relates to the coefficient of heat transfer associated with warm fluid. Thus, if the thermal Biot number rises, the hot fluid side convection resistance falls, and as a result, the temperature rises. Fig. 15 is indicated to present the variation in temperature profile via Eckert number w.r.t. nanofluid and hybrid nanofluid. We conclude that temperature profile $\theta(\eta)$ is highlighted for amplifying values of Ec in both cases. As Ec is increased, additional heat is produced due to friction and hence the temperature profile rises. Fig. 16 depict the influence of thermal radiation parameter N on temperature distribution $\theta(\eta)$ for nanofluid and hybrid nanofluid. A direct relation is found between $\theta(\eta)$ and N everywhere in the boundary layer region for both cases. In view of physics, the mean

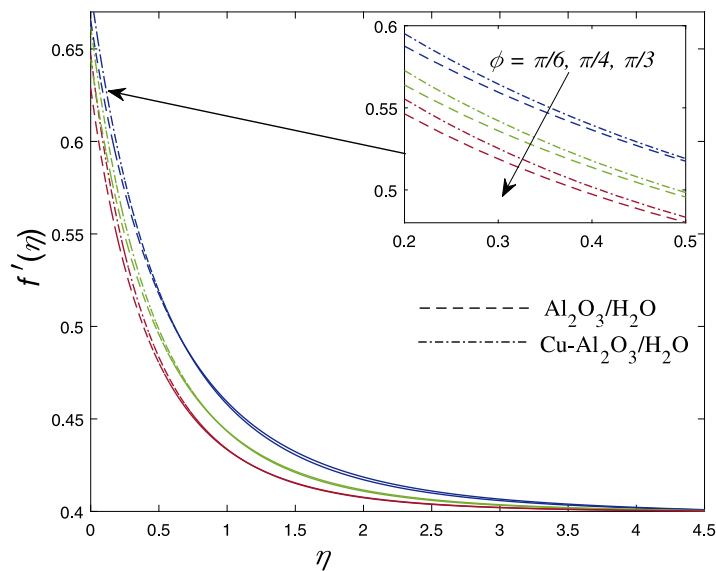


Fig. 8. Depiction of $f'(\eta)$ for altered values of ϕ .

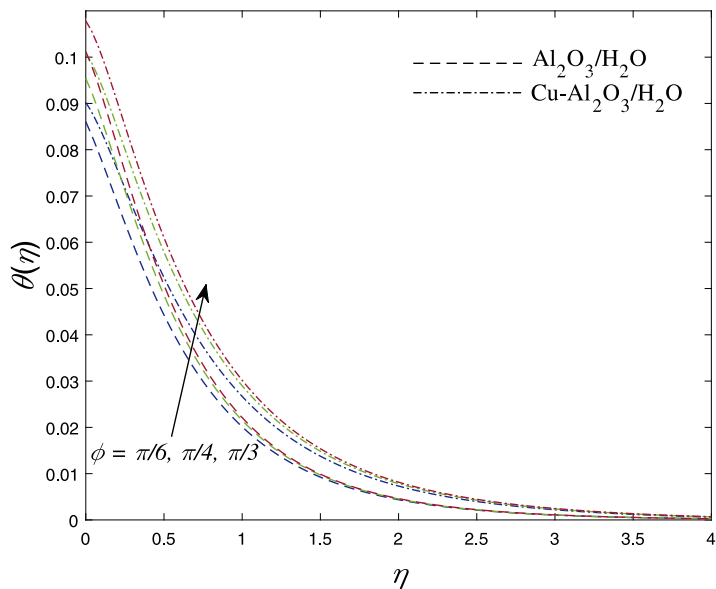


Fig. 9. Depiction of $\theta(\eta)$ for altered values of ϕ .

absorption coefficient decreases as the thermal radiation parameter increase. As a result, the temperature profile is improved. Fig. 17 displays the temperature distribution $\theta(\eta)$ under the influence of heat generation parameter Q w.r.t. nanofluid and hybrid nanofluid. For higher values of the heat generation parameter, we observe the increasing trend in temperature profiles in both cases. In the presence of heat generation parameter, some extra heat is added to the system and due to this, fluid temperature is improved.

Table 5 shows the variations in skin friction for the current fluid flow problem w.r.t. various controlling parameters for both nanofluid as well as hybrid nanofluid. It is clearly noticed from the table that the absolute value of local skin friction coefficient is an increasing function of A , M , ϕ and Φ_1 . In contrast, an opposite nature is perceived for the parameters λ_1 , δ and Gr for both the cases. Table 6 presents the variations of local Nusselt number w.r.t. various controlling parameters for nanofluid and hybrid nanofluid cases. Further, the table reveals that the local Nusselt number measuring the rate of heat transfer at the boundary is improved as the strength of physical parameters A , λ_1 , γ and N are escalated. On the other hand, a contrary behavior of heat transfer rate is noticed w.r.t. M , ϕ , Φ_1 , Ec and Q in both cases.

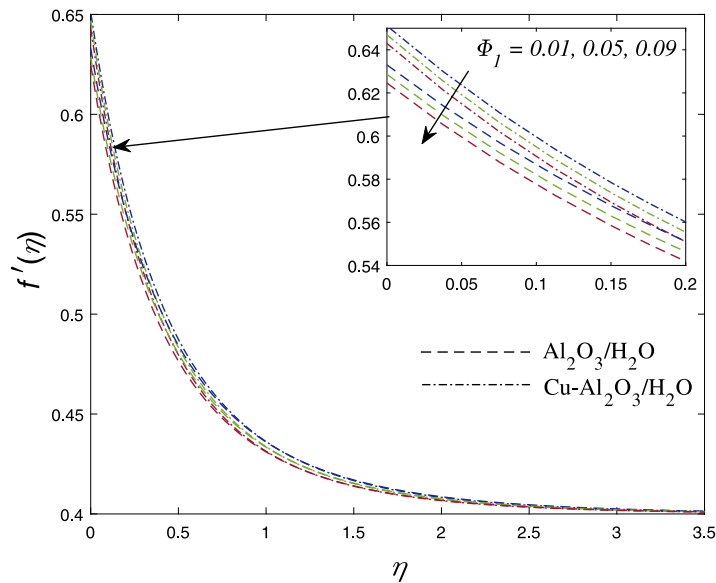


Fig. 10. Depiction of $f'(\eta)$ for altered values of Φ_1 .

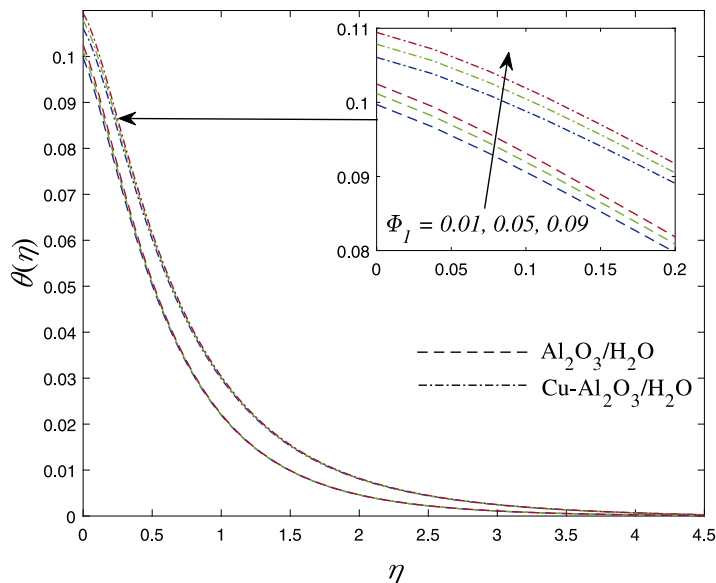


Fig. 11. Depiction of $\theta(\eta)$ for altered values of Φ_1 .

5. Quadratic regression model

In this section, the multiple (quadratic) regression model has been used to estimate the local skin friction coefficient and local Nusselt number. The values of M and δ are picked from the set of 200 values within the intervals $[1, 5]$ and $[0.1, 0.7]$ respectively to perform the quadratic regression analysis for the local skin friction coefficient w.r.t. altered values of A keeping the other parameters' values fixed. Similarly, the values of N and Ec are taken from the set of 200 values within the intervals $[0.2, 1.8]$ and $[0.1, 0.5]$ respectively to estimate the local Nusselt number using the quadratic regression model w.r.t. different values of γ while the other parameters are fixed. The values of the estimated skin friction coefficient ($C_{f_r Est.}$) w.r.t. M , δ and Nusselt number ($Nu_{r Est.}$) w.r.t. N , Ec are computed using the following quadratic regression models (see, Refs. [61,62]):

$$C_{f_r Est.} = C_f + \kappa_1 M + \kappa_2 \delta + \kappa_3 M^2 + \kappa_4 \delta^2 + \kappa_5 M \delta, \tag{15}$$

$$Nu_{r Est.} = Nu + \psi_1 N + \psi_2 Ec + \psi_3 N^2 + \psi_4 Ec^2 + \psi_5 N Ec, \tag{16}$$

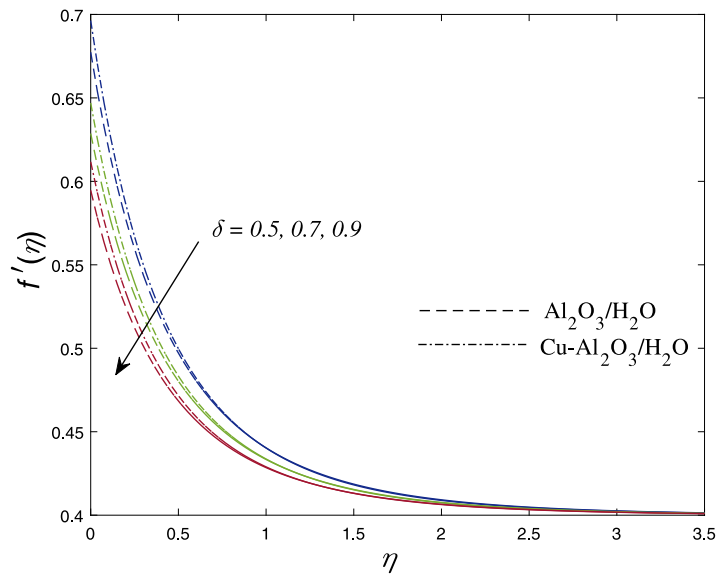


Fig. 12. Depiction of $f'(\eta)$ for altered values of δ .

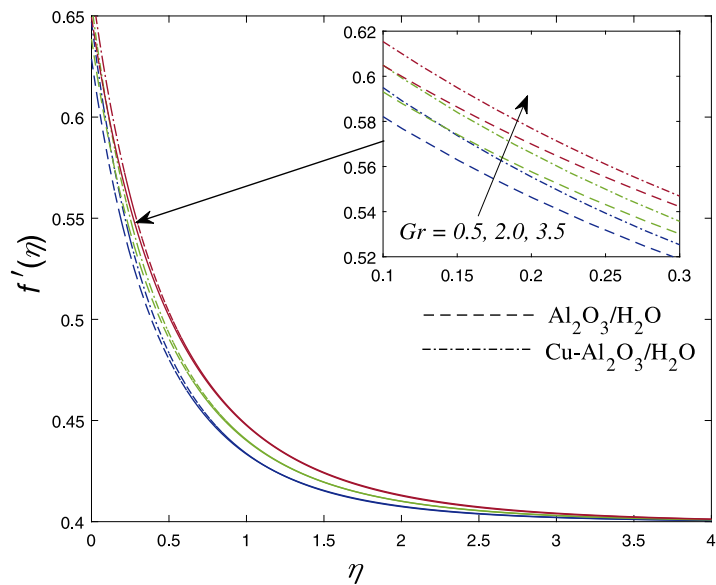


Fig. 13. Depiction of $f'(\eta)$ for altered values of Gr .

where $C_f = -C_{f_r} Re_x^{1/2}$ and $N_u = Nu_r Re_x^{-1/2}$ while κ_i, ψ_i ($i = 1, 2, \dots, 5$) denote the regression coefficients.

The greatest relative error ϵ_1 for local skin friction coefficient and ϵ_2 local Nusselt number is calculated using the following formulae (see, Refs. [61,62]):

$$\epsilon_1 = \frac{|C_{f_r Est.} - C_f|}{|C_f|} \quad \text{and} \quad \epsilon_2 = \frac{|Nu_r Est. - Nu|}{|Nu|}. \tag{17}$$

The quadratic regression coefficients for the local skin friction coefficient estimation and the maximum relative error are presented in Table 7. It is clear from the table that for rising values of A , the regression coefficient of δ is higher compared to the regression coefficient of M in absolute value-form. This implies that the impact of δ is more dominant on the local surface drag coefficient in comparison to M . Similarly, the quadratic regression coefficients of the local Nusselt number estimation and the maximum relative error are shown in Table 8. It is observed that the regression coefficient of N is larger compared to the regression coefficient of Ec for amplifying values of γ . Hence, N is more dominant on local Nusselt number compared to Ec .

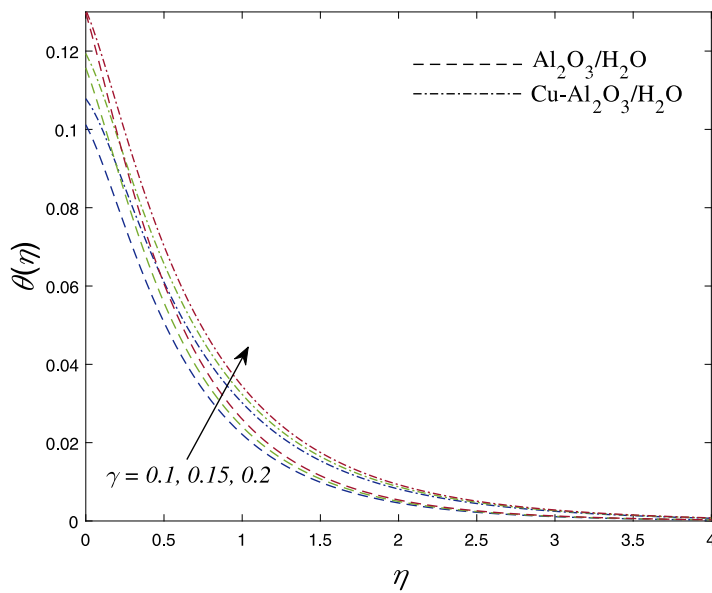


Fig. 14. Depiction of $\theta(\eta)$ for altered values of γ .

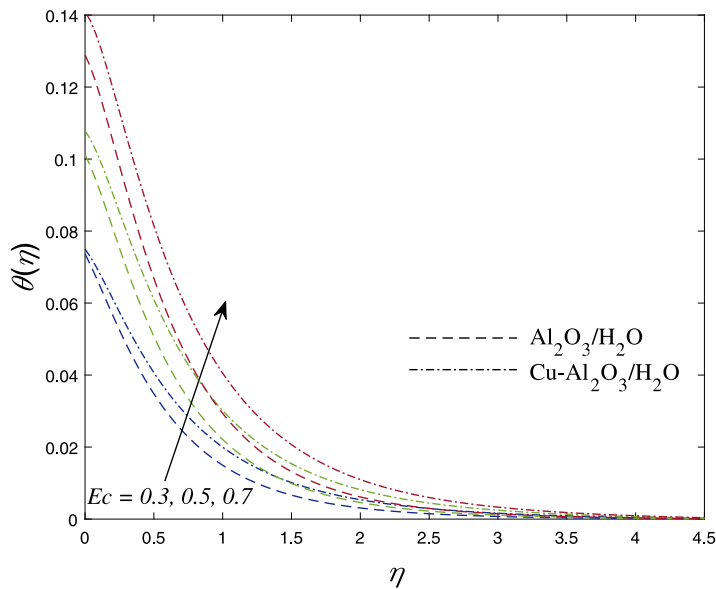


Fig. 15. Depiction of $\theta(\eta)$ for altered values of Ec .

6. Conclusions

The present study focuses on the unsteady stagnation flow of Cu-Al₂O₃/H₂O hybrid nanofluid past a convectively heated stretching cylinder under the influence of oblique Lorentz force. The aspects of velocity slip at the wall, Joule dissipation, thermal radiation, viscous dissipation and internal heat source are also taken into consideration. As the governing equations are highly nonlinear in nature, Runge–Kutta–Fehlberg method-based shooting technique has been employed to obtain the numerical solutions for the momentum and thermal fields. The noticeable outcomes of this study are stated below:

- Angle of inclination of the magnetic field tends to retard the hybrid nanofluid flow. Also, the unsteadiness in the flow-field causes a substantial reduction in the fluid velocity.
- Thermal buoyancy force boosts the flow whereas a contrary impact is reported for the magnetic field and the velocity slip at the wall.

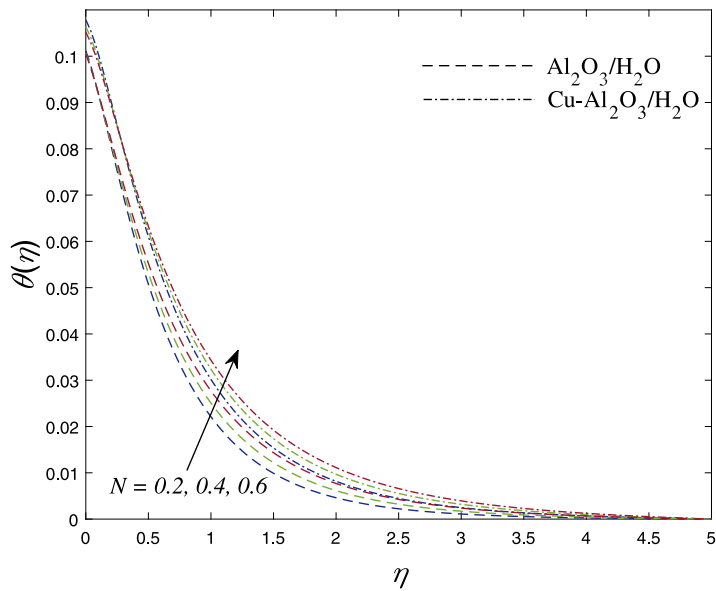


Fig. 16. Depiction of $\theta(\eta)$ for altered values of N .

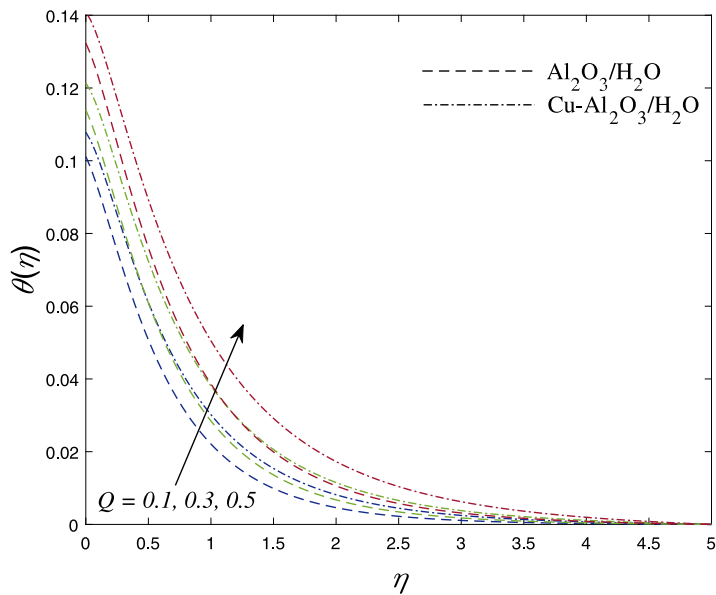


Fig. 17. Depiction of $\theta(\eta)$ for altered values of Q .

- The viscous dissipation, radiation and internal heat source have the tendency to escalate the fluid temperature. However, opposite effect is seen w.r.t. unsteadiness parameter.
- The skin-friction at the surface of the cylinder is intensified as the strength of unsteadiness and magnetic field is improved. But, the buoyancy force and the slip at the boundary reduce the wall skin-friction.
- There is a significant reduction in heat transfer rate at the surface upon improvement in magnetic strength and viscous dissipation while Biot number, thermal radiation and unsteadiness parameters uplift the heat transfer rate at the surface.
- The quadratic regression analysis reveals that skin friction is more prone to velocity slip parameter than the magnetic parameter. However, the Nusselt number is more sensitive to the radiation parameter as compared to the Eckert number.

We have examined various aspects of the physical problem under the assumption in the present work. But, still, there is the scope of extending the work further. One can extend the work by considering this problem for a different geometry (rotating disk, thin needle, etc.).

Table 5
Numerical values of $C_f Re_x^{1/2}$ for different governing parameters.

A	λ_1	M	ϕ	Φ_1	δ	Gr	$C_f Re_x^{1/2}$	
							Al ₂ O ₃ /H ₂ O	Cu-Al ₂ O ₃ /H ₂ O
0.5	0.4	5.0	$\pi/3$	0.05	0.7	0.5	1.219148	1.553182
2.5	0.4	5.0	$\pi/3$	0.05	0.7	0.5	1.283244	1.647346
4.5	0.4	5.0	$\pi/3$	0.05	0.7	0.5	1.329856	1.715775
0.5	0.6	5.0	$\pi/3$	0.05	0.7	0.5	0.827068	1.056454
0.5	0.8	5.0	$\pi/3$	0.05	0.7	0.5	0.419214	0.536931
0.5	0.4	7.0	$\pi/3$	0.05	0.7	0.5	1.267830	1.617035
0.5	0.4	9.0	$\pi/3$	0.05	0.7	0.5	1.306757	1.668930
0.5	0.4	5.0	$\pi/6$	0.05	0.7	0.5	1.098818	1.400885
0.5	0.4	5.0	$\pi/4$	0.05	0.7	0.5	1.167289	1.486531
0.5	0.4	5.0	$\pi/3$	0.01	0.7	0.5	1.204897	1.534720
0.5	0.4	5.0	$\pi/3$	0.09	0.7	0.5	1.232472	1.570538
0.5	0.4	5.0	$\pi/3$	0.09	0.5	0.5	1.483009	1.870128
0.5	0.4	5.0	$\pi/3$	0.09	0.9	0.5	1.035195	1.328463
0.5	0.4	5.0	$\pi/3$	0.09	0.4	2.0	1.186346	1.514187
0.5	0.4	5.0	$\pi/3$	0.09	0.4	3.5	1.150925	1.472706

Table 6
Numerical values of $Nu_r Re_x^{-1/2}$ for different governing parameters.

A	λ_1	M	ϕ	Φ_1	γ	Ec	N	Q	$Nu_r Re_x^{-1/2}$	
									Al ₂ O ₃ /H ₂ O	Cu-Al ₂ O ₃ /H ₂ O
0.5	0.4	5.0	$\pi/3$	0.05	0.1	0.5	0.2	0.1	0.104138	0.098771
2.5	0.4	5.0	$\pi/3$	0.05	0.1	0.5	0.2	0.1	0.109316	0.104061
4.5	0.4	5.0	$\pi/3$	0.05	0.1	0.5	0.2	0.1	0.111103	0.105904
0.5	0.6	5.0	$\pi/3$	0.05	0.1	0.5	0.2	0.1	0.100150	0.094330
0.5	0.8	5.0	$\pi/3$	0.05	0.1	0.5	0.2	0.1	0.107127	0.102103
0.5	0.4	7.0	$\pi/3$	0.05	0.1	0.5	0.2	0.1	0.103631	0.098172
0.5	0.4	9.0	$\pi/3$	0.05	0.1	0.5	0.2	0.1	0.103314	0.097783
0.5	0.4	5.0	$\pi/6$	0.05	0.1	0.5	0.2	0.1	0.105891	0.100725
0.5	0.4	5.0	$\pi/4$	0.05	0.1	0.5	0.2	0.1	0.104809	0.099536
0.5	0.4	5.0	$\pi/3$	0.01	0.1	0.5	0.2	0.1	0.104309	0.098969
0.5	0.4	5.0	$\pi/3$	0.09	0.1	0.5	0.2	0.1	0.103988	0.098595
0.5	0.4	5.0	$\pi/3$	0.09	0.15	0.5	0.2	0.1	0.153682	0.146244
0.5	0.4	5.0	$\pi/3$	0.09	0.2	0.5	0.2	0.1	0.201649	0.192508
0.5	0.4	5.0	$\pi/3$	0.09	0.1	0.3	0.2	0.1	0.107327	0.102408
0.5	0.4	5.0	$\pi/3$	0.09	0.1	0.7	0.2	0.1	0.100928	0.095114
0.5	0.4	5.0	$\pi/3$	0.09	0.1	0.7	0.4	0.1	0.125594	0.113297
0.5	0.4	5.0	$\pi/3$	0.09	0.1	0.7	0.6	0.1	0.147006	0.127820
0.5	0.4	5.0	$\pi/3$	0.09	0.1	0.7	0.6	0.3	0.102657	0.097270
0.5	0.4	5.0	$\pi/3$	0.09	0.1	0.7	0.6	0.5	0.100525	0.095109

Table 7
Quadratic regression coefficients and error bound of $-C_f Re_x^{1/2}$ w.r.t. A.

A	C_f	κ_1	κ_2	κ_3	κ_4	κ_5	ϵ_1
0.5	2.7482	0.2159	-3.8682	-0.0117	2.5684	-0.1559	0.0062
2.5	3.3275	0.1993	-5.0440	-0.0118	3.3210	-0.1341	0.0091
4.5	3.9390	0.1139	-6.2757	0.0023	4.6414	-0.2039	0.0095

Table 8
Quadratic regression coefficients and error bound of $Nu_r Re_x^{-1/2}$ w.r.t. γ .

γ	N_u	ψ_1	ψ_2	ψ_3	ψ_4	ψ_5	ϵ_2
0.1	0.0976	0.0513	-0.0172	-0.0001	0.0001	-0.0053	0.00013
0.3	0.2794	0.1421	-0.0500	-0.0015	0.0006	-0.0138	0.00009
0.5	0.4452	0.2196	-0.0799	-0.0037	0.0009	-0.0209	0.00015

Declaration of competing interest

The authors declare that they have no known competing financial interests or personal relationships that could have appeared to influence the work reported in this paper.

Acknowledgment

The first author is very much thankful to the National Institute of Technology Meghalaya for providing all kinds of facilities to carry out this research.

References

- [1] S.S.C. Ghadikolaei, Solar photovoltaic cells performance improvement by cooling technology: An overall review, *Int. J. Hydrogen Energy* 46 (18) (2021) 10939–10972, <http://dx.doi.org/10.1016/j.ijhydene.2020.12.164>.
- [2] S.S. Ghadikolaei, K. Hosseinzadeh, M. Hatami, D.D. Ganji, M. Armin, Investigation for squeezing flow of ethylene glycol (C₂H₆O₂) carbon nanotubes (CNTs) in rotating stretching channel with nonlinear thermal radiation, *J. Molecular Liquids* 263 (2018) 10–21, <http://dx.doi.org/10.1016/j.molliq.2018.04.141>.
- [3] S.S.C. Ghadikolaei, An enviroeconomic review of the solar PV cells cooling technology effect on the CO₂ emission reduction, *Sol. Energy* 216 (2021) 468–492, <http://dx.doi.org/10.1016/j.solener.2021.01.016>.
- [4] Hashim, A. Hamid, M. Khan, Heat and mass transport phenomena of nanoparticles on time-dependent flow of Williamson fluid towards heated surface, *Neural Comput. Appl.* 32 (2018) 3253–3263, <http://dx.doi.org/10.1007/s00521-019-04100-4>.
- [5] S. Dinarvand, M.N. Rostami, I. Pop, A novel hybridity model for TiO₂-CuO/water hybrid nanofluid flow over a static/moving wedge or corner, *Sci. Rep.* 9 (2019) 16290, <http://dx.doi.org/10.1038/s41598-019-52720-6>.
- [6] I. Waini, A. Ishak, I. Pop, Unsteady flow and heat transfer past a stretching/shrinking sheet in a hybrid nanofluid, *Int. J. Heat Mass Transfer* 136 (2020) 288–297, <http://dx.doi.org/10.1016/j.ijheatmasstransfer.2019.02.101>.
- [7] E.H. Aly, I. Pop, Merkin and needham wall jet problem for hybrid nanofluids with thermal energy, *Eur. J. Mech. / B Fluids* 83 (2020) 195–204, <http://dx.doi.org/10.1016/j.euromechflu.2020.05.004>.
- [8] A.A.A. Arani, H. Aberoumand, Stagnation-point flow of Ag-CuO/water hybrid nanofluids over a permeable stretching/shrinking sheet with temporal stability analysis, *Powder Technol.* 380 (2020) 152–163, <http://dx.doi.org/10.1016/j.powtec.2020.11.043>.
- [9] I. Waini, A. Ishak, I. Pop, Hybrid nanofluid flow towards a stagnation point on a stretching/shrinking cylinder, *Sci. Rep.* 10 (2020) 9296, <http://dx.doi.org/10.1038/s41598-020-66126-2>.
- [10] A. Hamid, Hashim, M. Khan, A. Hafeez, Unsteady stagnation-point flow of williamson fluid generated by stretching/shrinking sheet with Ohmic heating, *Int. J. Heat Mass Transfer* 126 (2018) 933–940, <http://dx.doi.org/10.1016/j.ijheatmasstransfer.2018.05.076>.
- [11] S.S. Ghadikolaei, M. Yassari, H. Sadeghi, K. Hosseinzadeh, D.D. Ganji, Investigation on thermophysical properties of TiO₂-Cu/H₂O hybrid nanofluid transport dependent on shape factor in MHD stagnation point flow, *Powder Technol.* 322 (2017) 428–438, <http://dx.doi.org/10.1016/j.powtec.2017.09.006>.
- [12] A. Hamid, Hashim, M. Khan, A.S. Alshomrani, M. Alghamdi, Heat transport features of magnetic water-graphene oxide nanofluid flow with thermal radiation: Stability test, *Eur. J. Mech. B/Fluids* 76 (2019) 434–441, <http://dx.doi.org/10.1016/j.euromechflu.2019.04.008>.
- [13] N.A. Zainal, R. Nazar, K. Naganthran, I. Pop, Unsteady three-dimensional MHD non-axisymmetric homann stagnation point flow of a hybrid nanofluid with stability analysis, *Mathematics* 8 (2020) 784, <http://dx.doi.org/10.3390/math8050784>.
- [14] A. Jamaludin, K. Naganthran, R. Nazar, I. Pop, MHD mixed convection stagnation-point flow of Cu-Al₂O₃/water hybrid nanofluid over a permeable stretching/shrinking surface with heat source/sink, *Eur. J. Mech. / B Fluids* 84 (2020) 71–80, <http://dx.doi.org/10.1016/j.euromechflu.2020.05.017>.
- [15] N.A. Zainal, R. Nazar, K. Naganthran, I. Pop, Stability analysis of MHD hybrid nanofluid flow over a stretch- ing/shrinking sheet with quadratic velocity, *Alex. Eng. J.* 60 (2021) 915–926, <http://dx.doi.org/10.1016/j.aej.2020.10.020>.
- [16] T. Srinivasulu, B.S. Goud, Effect of inclined magnetic field on flow, heat and mass transfer of williamson nanofluid over a stretching sheet, *Case Stud. Therm. Eng.* 23 (2021) 100819, <http://dx.doi.org/10.1016/j.csite.2020.100819>.
- [17] M.F.M. Basir, M.J. Uddin, A.I.M. Ismail, O.A. Bég, Nanofluid slip flow over a stretching cylinder with Schmidt and Péclet number effects, *AIP Adv.* 6 (2016) 055316, <http://dx.doi.org/10.1063/1.4951675>.
- [18] G. Degavath, N. Kishan, Velocity and curvature slip impacts on casson nanofluid flow over an inclined magnetic permeable stretching cylinder, *J. Nanofluids* 8 (4) (2019) 830–837, <http://dx.doi.org/10.1166/jon.2019.1630>.
- [19] A.S. Alshomrani, M. Ramzan, Upshot of magnetic dipole on the flow of nanofluid along a stretched cylinder with gyrotactic microorganism in a stratified medium, *Phys. Scr.* 95 (2) (2019) 025702, <http://dx.doi.org/10.1088/1402-4896/ab4067>.
- [20] A. Hamid, M. Khan, M. Alghamdi, Numerical simulation for transient flow of williamson fluid with multiple slip model in the presence of chemically reacting species, *Internat. J. Numer. Methods Heat Fluid Flow* 29 (11) (2019) 4445–4461, <http://dx.doi.org/10.1108/HFF-02-2019-0151>.
- [21] I. Tlili, H.A. Nabwey, G.P. Ashwinkumar, N. Sandeep, 3-D magnetohydrodynamic AA7072-AA7075/methanol hybrid nanofluid flow above an uneven thickness surface with slip effect, *Sci. Rep.* 10 (2020) 4265, <http://dx.doi.org/10.1038/s41598-020-61215-8>.
- [22] N. Abbas, S. Nadeem, A. Saleem, M.Y. Malik, A. Issakhov, F.M. Alharbi, Models base study of inclined MHD of hybrid nanofluid flow over nonlinear stretching cylinder, *Chinese J. Phys.* 69 (2021) 109–117, <http://dx.doi.org/10.1016/j.cjph.2020.11.019>.
- [23] A. Hussain, M.Y. Malik, T. Salahuddin, S. Bilal, M. Awais, Combined effects of viscous dissipation and joule heating on mhd sisko nanofluid over a stretching cylinder, *J. Molecular Liquids* 231 (2017) 341–352, <http://dx.doi.org/10.1016/j.molliq.2017.02.030>.
- [24] S.S. Ghadikolaei, K. Hosseinzadeh, M. Yassari, H. Sadeghi, D.D. Ganji, Analytical and numerical solution of non-Newtonian second-grade fluid flow on a stretching sheet, *Therm. Sci. Eng. Prog.* 5 (2017) 309–316, <http://dx.doi.org/10.1016/j.tsep.2017.12.010>.
- [25] M.M. Maskeen, A. Zeeshan, O.U. Mehmood, M. Hassan, Heat transfer enhancement in hydromagnetic alumina-copper/water hybrid nanofluid flow over a stretching cylinder, *J. Therm. Anal. Calorim.* 138 (2019) 1127–1136, <http://dx.doi.org/10.1007/s10973-019-08304-7>.
- [26] Z. Shah, E.O. Alzahrani, W. Alghamdi, M.Z. Ullah, Influences of electrical MHD and hall current on squeezing nanofluid flow inside rotating porous plates with viscous and joule dissipation effects, *J. Therm. Anal. Calorim.* 140 (2020) 1215–1227, <http://dx.doi.org/10.1007/s10973-019-09176-7>.
- [27] A. Tassaddiq, Impact of Cattaneo-Christov heat flux model on MHD hybrid nano-micropolar fluid flow and heat transfer with viscous and joule dissipation effects, *Sci. Rep.* 11 (2021) 67, <http://dx.doi.org/10.1038/s41598-020-77419-x>.
- [28] S.S. Ghadikolaei, K. Hosseinzadeh, D.D. Ganji, B. Jafari, Nonlinear thermal radiation effect on magneto Casson nanofluid flow with Joule heating effect over an inclined porous stretching sheet, *Case Stud. Therm. Eng.* 12 (2018) 176–187, <http://dx.doi.org/10.1016/j.csite.2018.04.009>.
- [29] S.S. Ghadikolaei, K. Hosseinzadeh, D.D. Ganji, Investigation on Magneto Eyring-Powell nanofluid flow over inclined stretching cylinder with nonlinear thermal radiation and Joule heating effect, *World J. Eng.* 16 (2019) 51–63, <http://dx.doi.org/10.1108/WJE-06-2018-0204>.
- [30] A. Mishra, A.K. Pandey, M. Kumar, Ohmic-viscous dissipation and slip effects on nanofluid flow over a stretching cylinder with suction/injection, *Nanosci. Technol.: Int. J.* 9 (2) (2018) 99–115, <http://dx.doi.org/10.1615/NanoSciTechnolIntJ.2018025410>.

- [31] Hashim, A. Hamid, M. Khan, Unsteady mixed convective flow of Williamson nanofluid with heat transfer in the presence of variable thermal conductivity and magnetic field, *J. Molecular Liquids* 260 (2018) 436–446, <http://dx.doi.org/10.1016/j.molliq.2018.03.079>.
- [32] A. Hamid, Hashim, M. Khan, Impacts of binary chemical reaction with activation energy on unsteady flow of magneto-Williamson nanofluid, *J. Molecular Liquids* 262 (2018) 435–442, <http://dx.doi.org/10.1016/j.molliq.2018.04.095>.
- [33] A. Mishra, M. Kumar, Velocity and thermal slip effects on MHD nanofluid flow past a stretching cylinder with viscous dissipation and Joule heating, *SN Appl. Sci.* 2 (8) (2020) 1–13, <http://dx.doi.org/10.1007/s42452-020-3156-7>.
- [34] F. Mabood, I. Tlili, A. Shafiq, Features of inclined magnetohydrodynamics on a second-grade fluid impinging on vertical stretching cylinder with suction and Newtonian heating, *Math. Methods Appl. Sci.* (2020) <http://dx.doi.org/10.1002/mma.6489>.
- [35] K. Singh, A.K. Pandey, M. Kumar, Melting heat transfer assessment on magnetic nanofluid flow past a porous stretching cylinder, *J. Egypt. Math. Soc.* 29 (2021) 1, <http://dx.doi.org/10.1186/s42787-020-00109-0>.
- [36] N.S. Wahid, N.M. Arifin, N.S. Khashi'ie, I. Pop, Hybrid nanofluid slip flow over an exponentially stretching/shrinking permeable sheet with heat generation, *Mathematics* 9 (1) (2021) 30, <http://dx.doi.org/10.3390/math9010030>.
- [37] S.S. Ghadikolaei, K. Hosseinzadeh, D.D. Ganji, Analysis of unsteady MHD Eyring-Powell squeezing flow in stretching channel with considering thermal radiation and joule heating effect using AGM, *Case Stud. Therm. Eng.* 10 (2017) 579–594, <http://dx.doi.org/10.1016/j.csite.2017.11.004>.
- [38] S.S. Ghadikolaei, K. Hosseinzadeh, M. Yassari, H. Sadeghi, D.D. Ganji, Boundary layer analysis of micropolar dusty fluid with TiO₂ nanoparticles in a porous medium under the effect of magnetic field and thermal radiation over a stretching sheet, *J. Molecular Liquids* 244 (2017) 374–389, <http://dx.doi.org/10.1016/j.molliq.2017.08.111>.
- [39] S.S. Ghadikolaei, K. Hosseinzadeh, D.D. Ganji, M. Hatami, Fe₃O₄-(CH₂OH)₂ nanofluid analysis in a porous medium under MHD radiative boundary layer and dusty fluid, *J. Molecular Liquids* 258 (2018) 172–185, <http://dx.doi.org/10.1016/j.molliq.2018.02.106>.
- [40] S.S. Ghadikolaei, K. Hosseinzadeh, M. Hatami, D.D. Ganji, MHD boundary layer analysis for micropolar dusty fluid containing Hybrid nanoparticles (Cu-Al₂O₃) over a porous medium, *J. Molecular Liquids* 268 (2018) 813–823, <http://dx.doi.org/10.1016/j.molliq.2018.07.105>.
- [41] N. Acharya, K. Das, P.K. Kundu, Framing the features of MHD boundary layer flow past an unsteady stretching cylinder in presence of non-uniform heat source, *J. Molecular Liquids* 225 (2017) 418–425, <http://dx.doi.org/10.1016/j.molliq.2016.11.085>.
- [42] A.K. Pandey, M. Kumar, Boundary layer flow and heat transfer analysis on Cu-water nanofluid flow over a stretching cylinder with slip, *Alex. Eng. J.* 56 (2017) 671–677, <http://dx.doi.org/10.1016/j.aej.2017.01.017>.
- [43] A. Zeeshan, M.M. Maskeen, O.U. Mehmood, Hydromagnetic nanofluid flow past a stretching cylinder embedded in non-Darcian Forchheimer porous media, *Neural Comput. Appl.* 30 (2018) 3479–3489, <http://dx.doi.org/10.1007/s00521-017-2934-7>.
- [44] S.S. Ghadikolaei, K. Hosseinzadeh, D.D. Ganji, Investigation on ethylene glycol-water mixture fluid suspend by hybrid nanoparticles (TiO₂-CuO) over rotating cone with considering nanoparticles shape factor, *J. Molecular Liquids* 272 (2018) 226–236, <http://dx.doi.org/10.1016/j.molliq.2018.09.084>.
- [45] S.S. Ghadikolaei, K. Hosseinzadeh, D.D. Ganji, Numerical study on magnetohydrodynamic CNTs-water nanofluids as a micropolar dusty fluid influenced by non-linear thermal radiation and joule heating effect, *Powder Technol.* 340 (2018) 389–399, <http://dx.doi.org/10.1016/j.powtec.2018.09.023>.
- [46] V. Vinita, V. Poply, Impact of outer velocity MHD slip flow and heat transfer of nanofluid past a stretching cylinder, *Mater. Today: Proc.* 26 (2019) 3429–3435, <http://dx.doi.org/10.1016/j.matpr.2019.11.304>.
- [47] S.S. Ghadikolaei, M. Gholinia, M.E. Hoseini, D.D. Ganji, Natural convection MHD flow due to MoS₂-Ag nanoparticles suspended in C₂H₆O₂-H₂O hybrid base fluid with thermal radiation, *J. Taiwan Inst. Chem. Eng.* 97 (2019) 12–23, <http://dx.doi.org/10.1016/j.jtice.2019.01.028>.
- [48] A. Hamid, Hashim, M. Alghamdi, M. Khan, A.S. Alshomrani, An investigation of thermal and solutal stratification effects on mixed convection flow and heat transfer of Williamson nanofluid, *J. Molecular Liquids* 284 (2019) 307–315, <http://dx.doi.org/10.1016/j.molliq.2019.03.181>.
- [49] Vinita, V. Poply, R. Goyal, N. Sharma, Analysis of the velocity, thermal, and concentration MHD slip flow over a nonlinear stretching cylinder in the presence of outer velocity, *Heat Transfer* 50 (2) (2020) 1543–1569, <http://dx.doi.org/10.1002/htj.21941>.
- [50] I. Khan, Shafquatullah, M.Y. Malik, A. Hussain, M. Khan, Magnetohydrodynamics Carreau nanofluid flow over an inclined convective heated stretching cylinder with Joule heating, *Results Phys.* 7 (2017) 4001–4012, <http://dx.doi.org/10.1016/j.rinp.2017.10.015>.
- [51] N.A.A. Bakar, N. Bachok, N.M. Arifin, I. Pop, Stability analysis on the flow and heat transfer of nanofluid past a stretching/shrinking cylinder with suction effect, *Results Phys.* 9 (2018) 1335–1344, <http://dx.doi.org/10.1016/j.rinp.2018.04.056>.
- [52] S.S. Ghadikolaei, M. Gholinia, Terrific effect of H₂ on 3D free convection MHD flow of C₂H₆O₂-H₂O hybrid base fluid to dissolve Cu nanoparticles in a porous space considering the thermal radiation and nanoparticle shapes effects, *Int. J. Hydrogen Energy* 44 (31) (2019) 17072–17083, <http://dx.doi.org/10.1016/j.ijhydene.2019.04.171>.
- [53] N.S. Khashi'ie, N.M. Arifin, I. Pop, R. Nazari, E.H. Hafidzuddin, N. Wahi, Three-dimensional hybrid nanofluid flow and heat transfer past a permeable stretching/shrinking sheet with velocity slip and convective condition, *Chinese J. Phys.* 66 (2020) 157–171, <http://dx.doi.org/10.1016/j.cjph.2020.03.032>.
- [54] S.S. Ghadikolaei, M. Gholinia, 3D mixed convection MHD flow of GO-MoS₂ hybrid nanoparticles in H₂O-(CH₂OH)₂ hybrid base fluid under the effect of H₂ bond, *Int. Commun. Heat Mass Transfer* 110 (2020) 104371, <http://dx.doi.org/10.1016/j.icheatmasstransfer.2019.104371>.
- [55] N.S. Anuar, N. Bachok, I. Pop, Cu-Al₂O₃/Water hybrid nanofluid stagnation point flow past MHD stretching/shrinking sheet in presence of homogeneous-heterogeneous and convective boundary conditions, *Mathematics* 8 (8) (2020) 1237, <http://dx.doi.org/10.3390/math8081237>.
- [56] A. Hussain, M.H. Alshbool, A. Abdussattar, A. Rehman, H. Ahmad, T.A. Nofal, M.R. Khan, A computational model for hybrid nanofluid flow on a rotating surface in the existence of convective condition, *Case Stud. Therm. Eng.* 26 (2021) 101089, <http://dx.doi.org/10.1016/j.csite.2021.101089>.
- [57] A. Hamid, Existence of dual solutions for wedge flow of magneto-Williamson nanofluid: A revised model, *Alex. Eng. J.* 59 (3) (2020) 1525–1537, <http://dx.doi.org/10.1016/j.aej.2020.04.001>.
- [58] S.S. Ghadikolaei, M. Yassari, H. Sadeghi, K. Hosseinzadeh, D.D. Ganji, Investigation on thermophysical properties of TiO₂-Cu/H₂O hybrid nanofluid transport dependent on shape factor in MHD stagnation point flow, *Powder Technol.* 322 (2017) 428–438, <http://dx.doi.org/10.1016/j.powtec.2017.09.006>.
- [59] B. Sahoo, Y. Do, Effects of slip on sheet-driven flow and heat transfer of a third grade fluid past a stretching sheet, *Int. Commun. Heat Mass Transfer* 37 (8) (2010) 1064–1071, <http://dx.doi.org/10.1016/j.icheatmasstransfer.2010.06.018>.
- [60] A. Noghrehabadi, R. Pourrajab, M. Ghalambaz, Effect of partial slip boundary condition on the flow and heat transfer of nanofluids past stretching sheet prescribed constant wall temperature, *Int. J. Therm. Sci.* 54 (2012) 253–261, <http://dx.doi.org/10.1016/j.ijthermalsci.2011.11.017>.
- [61] R. Sharma, S.M. Hussain, C.S.K. Raju, G.S. Seth, A.J. Chamkha, Study of graphene Maxwell nanofluid flow past a linearly stretched sheet: A numerical and statistical approach, *Chinese J. Phys.* 68 (2020) 671–683, <http://dx.doi.org/10.1016/j.cjph.2020.10.013>.
- [62] V.K. Sinha, B. Kumar, G.S. Seth, R. Nandkeolyar, Outlining the impact of thermal radiation on micropolar nanofluid viscous dissipative flow: A spectral method based numerical simulation with regression analysis, *AIP Conf. Proc.* 2253 (2020) 020024, <http://dx.doi.org/10.1063/5.0019259>.